ISSN 1070-3284, Russian Journal of Coordination Chemistry, 2014, Vol. 40, No. 12, pp. 932–942. © Pleiades Publishing, Ltd., 2014.

Syntheses, Crystal Structures, and Characterization of Copper(II) Carboxylate Complexes Incorporating *o*-Hydroxybenzoic Acid and *p*-Hydroxybenzoic Acid[1]

C. J. Lin, Y. Q. Zheng*, D. Y. Zhang, and W. Xu

Crystal Engineering Lab, Research Center for Solid State Chemistry & Application Ningbo University, Ningbo, 315211 P.R. China

**e-mail: yqzhengmc@163.com*

Received April 30, 2014

Abstract—Two new complexes, $[Cu(Phen)(o\text{-Hbza})(H_2O)_2][Cu(Phen)(o\text{-Hbza})Cl]_2(o\text{-Hbza})$ (**I**) and $[Cu(Phen)(H_2O)(p\text{-Hbza})Cl]\ H_2O$ (**II**) (*o*-Hbza = *o*-hydroxybenzoic acid, *p*-Hbza = *p*-hydroxybenzoic acid, Phen = 1,10-phenanthroline), have been synthesized and characterized by single-crystal X-ray diffraction methods (CIF files CCDC nos. 975524 (**I**) and 975525 (**II**)), elemental analyses, IR spectroscopy, thermal analyses as well as magnetic measurements. Compound **I** is extended into 1D chains through hydrogen-bonding and further assembled into 2D supramolecular layers through π···π interactions. Compound **II** is pairwise aggregated to form H-bonded dimuclear motifs, which are held together by π···π interactions into 1D chains and further assembled into 2D supramolecular networks by O–H···Cl hydrogen bonds. The magnetic behaviors of **I** and **II** obey the Curie–Weiss law with $\chi_m = C/(T - \theta)$ with the Curie constant C = 1.283(2) $cm^3\ mol^{-1}$ K and the Weiss constant θ = 0.284(4) K for **I**, as well as C = 0.424(1) $cm^3\ mol^{-1}$ K and θ = 0.040(4) K for **II**, indicating weak ferromagnetic interactions between the Cu^{2+} ions.

DOI: 10.1134/S1070328414120094

INTRODUCTON

Construction of supramolecular systems and crystal engineering have been one of the most active fields in supramolecular chemistry, coordination chemistry and materials science [1–3] due to their possible intriguing structural topologies and potential applications in host-guest chemistry, catalysis, separations, gas storage, optical properties and magnetic properties, etc. [4–8]. In the past decades, considerable effort has been devoted to design the supramolecular assemblies via hydrogen-bonding and π···π stacking interactions by carefully selecting building blocks and organic ligands in the field of supramolecular chemistry [9–11]. It is challenging to develop a new strategy based on hydrogen bonding for crystal engineering. The aggregation of smaller supramolecular units into larger arrays represents an actual approach to complicated organic assemblies and can lead to a new generation of solids with promising properties in catalysis, nonlinear optics, gas separation and molecular recognition [12–14]. Additionally, other supramolecular interactions, such as π···π and weak coordinative interactions, have also been well documented, and more and more examples generated by combination of multi supramolecular interactions have been reported. The groups of oxygen and nitrogen are the most common and simplest functional groups for hydrogen bonding. It is well known that carboxylates show variable bonding modes including monodentate, monodentate bridging, symmetric and asymmetric chelating, and bidentate. Our research has been dedicated to the exploration of *p*-hydroxybenzoic acid (*p*-Hbza) and *o*-hydroxybenzoic acid (*o*-Hbza) in combination with N-donor ligands, such as 1,10-phenanthroline (Phen), since the carboxylic acid can provide hydrogen-bond donors and acceptors and the heteroaromatic diimine ligands are sources for π···π stacking interactions [15, 16]. Structures containing Phen and monocarboxylic acid are typically of lower dimensionalities.

[1] The article is published in the original.

EXPERIMENTAL

Materials and physical methods. All chemicals of reagent grade were commercially available and used without further purification. Powder X-ray diffraction (PXRD) measurements were carried out with a Bruker D8 Focus X-ray diffractometer to check the phase purity. The C, N, and H microanalyses were performed with a PerkinElmer 2400II elemental analyzer. The FT-IR spectra were recorded from KBr pellets in the range 4000–400 cm^{-1} on a Shimadzu FTIR-8900 spectrometer. Thermogravimetric measurement was performed under a flow of nitrogen gas from room temperature to 900°C at a heating rate of 10°C/min using a Seiko Exstar 6000 TG/DTA 6300 apparatus.

Single crystal X-ray diffraction data were collected by Rigaku R-Axis Rapid X-ray diffractometer. The temperature-dependent magnetic susceptibilities were determined with a Quantum Design SQUID magnetomer (Quantum Design Model MPMS-7) in the temperature range 2–300 K with an applied field of 1 KOe, and diamagnetic corrections were estimated from Pascal's constants [17].

Synthesis of [Cu(Phen)(*o*-Hbza)(H_2O)$_2$][Cu(Phen)(*o*-Hbza)Cl]$_2$(*o*-Hbza) (I). $CuCl_2 \cdot 2H_2O$ (0.1730 g, 1.0 mmol), *o*-Hbza (0.1360 g, 1.0 mmol), Phen-monohydrate (0.1970 g, 1.0 mmol) and NaOH (0.0200 g, 0.5 mmol) were separately dissolved in mixed solvent of 5.0 mL H_2O and 5.0 mL CH_3OH. After dropwise addition of the organic acid solution to the Cu(II) solution, the Phen solution was added, during which the light blue solution turned gradually blue. Subsequently, the NaOH solution was dropwise added, and dissolution of the incipiently formed bluish flocculent precipitate on stirring afforded a dark blue solution (pH 3.12), which was then allowed to stand at room temperature for slow evaporation. About 6 days later, well-shaped blue crystals were grown in solution, and after separation, the product (the yield was ~52.7% on the basis of the initial *o*-Hbza input) was confirmed to be a pure phase by matching the experimental PXRD to the simulated one based on the single crystal data.

For $C_{64}H_{48}N_6O_{14}Cl_2Cu_3$

anal. calcd., %:	C, 55.44;	H, 3.49;	N, 6.06.
Found, %:	C, 55.23;	H, 3.26;	N, 6.24.

IR data (KBr; ν, cm^{-1}): 3447 w, 3065 w, 2924 w, 1624 m, 1583 s, 1560 s, 1517 s, 1485 s, 1450 s, 1389 v.s, 1256 s, 1220 w, 1140 s, 1107 w, 1030 m, 852 s, 758 s, 721 s, 667 s.

Synthesis of [Cu(Phen)(H_2O)(*p*-Hbza)Cl]H_2O (II) was carried out analogous to **I** except that *p*-Hbza (0.1410 g, 1.0 mmol) was used instead of *o*-Hbza. Slow evaporation of the resulting dark blue solution (pH 3.03) for 5 days afforded well-shaped blue crystals, and the product was finally separated in a high yield (~35% on the basis of the initial $CuCl_2 \cdot 2H_2O$ input) and verified to be a pure phase by comparing the experimental PXRD with the simulated one based on the single crystal data.

For $C_{19}H_{17}N_2O_5ClCu$

anal. calcd., %:	C, 50.45;	H, 3.79;	N, 6.19.
Found, %:	C, 50.31;	H, 3.62;	N, 6.31.

IR data (KBr; ν, cm^{-1}): 3169 m, 2673 w, 1595 v.s, 1541 v.s, 1520 s, 1506 v.w, 1425 w, 1389 v.s, 1283 s, 1242 s, 1163 s, 1101 m, 849 s, 789 s, 721 s, 700 w, 669 w, 636 m, 507 m.

X-ray crystallography. Suitable single crystals were selected under a polarizing microscope and fixed with epoxy cement on respective fine glass fibres, which were then mounted on a Rigaku R-Axis Rapid diffractomerter with graphite-monochromated MoK_α radiation (λ = 0.71073 Å) for cell determination and subsequent data collection. The reflection intensities in the suitable θ ranges were collected at 293 K using the ω scan technique. The employed single crystals exhibit no detectable decay during the data collection. The data were corrected for *Lp* and absorption effects. The direct method employing the SHELXS-97 program [18] gave the initial positions for part of non-hydrogen atoms, and the subsequent difference Fourier syntheses using SHELXL-97 program [19] resulted in initial positions for the rest non-hydrogen atoms. The hydrogen atoms attached to the carbon atoms were geometrically generated, while the remaining hydrogen atoms were located from the successive difference Fourier syntheses. The full-matrix least-squares technique was applied for refinement of positions and anisotropic displacement parameters of all the non-hydrogen atoms. Positions of the hydrogen atoms were refined using riding mode by fixing the initial distances to the associated heavier atoms with the isotropic displacement parameters set to 1.2 times of the values for the associated atoms. Detailed information about the crystal data and structure determination are summarized in Table 1. Selected interatomic distances and bond angles are given in Table 2. Hydrogen bonding contacts for **I** and **II** are listed in Table 3.

Supplementary material for structures **I** and **II** has been deposited with the Cambridge Crystallographic Data Centre (nos. 975524 (**I**), 975525 (**II**); deposit@ccdc.cam.ac.uk or http://www.ccdc.cam.ac.uk).

RESULTS AND DISCUSSION

The asymmetric unit of **I** consists of mononuclear [Cu(Phen)(*o*-Hbza)(H_2O)$_2$]$^+$ complex cation, dinuclear [Cu(Phen)(*o*-Hbza)Cl]$_2$ complex molecule, and (*o*-Hbza)$^-$ anion. As shown in Fig. 1a, within the mononuclear [Cu(Phen)(*o*-Hbza)(H_2O)$_2$]$^+$ complex cation, the Cu atom is coordinated by N(5), N(6) atoms of one Phen molecule, O(7) atom from *o*-hydroxybenzoate ligand, and O(10), O(11) atoms from two water molecules to form CuN_2O_3 chromophore. In the CuN_2O_3 coordination environment, N(5), N(6), O(7) and O(10) atoms locate in the corners of the basal plane and O(11) atom occupies the apical position. The radial Cu–N/O bond lengths fall in the regions 2.007(7)–2.020(3) and 1.950(2)–2.145(2) Å, and the cisoid and transoid angles around Cu atoms fall in the regions 81.0°–95.4° and 142.2°–171.9°, respectively, exhibiting significant departure from 90° to 180°. The Cu(3) atom exhibits the τ value of 0.496 [20] (τ = 0 for a perfect square pyramid, τ = 1 for a perfect trigonal bipyramid) indicates that the CuN_2O_3 core is a transition stage between the two ideal geometries. In the dinuclear [Cu(Phen)(*o*-

Table 1. Crystallographic data and structure refinement summary for **I** and **II**

Parameter	**I**	**II**
Formula mass	1386.63	452.35
Crystal system	Monoclinic	Triclinic
Space group	$P2_1/c$	$P\bar{1}$
a, Å	25.780(5)	7.7480(15)
b, Å	10.403(2)	10.668(2)
c, Å	22.493(5)	12.155(2)
α, deg	90.00	78.73(3)
β, deg	111.36(3)	87.65(3)
γ, deg	90.00	83.54(3)
Volume, Å^3	5618(2)	978.8(3)
Z	4	2
ρ_{calcd}, g cm^{-3}	1.639	1.535
F(000)	2828.0	462
μ, mm^{-1}	1.298	1.285
Reflections collected	53216	9641
Reflections with ($I \geq 2\sigma(I)$)	12878	4456
θ Range, deg	3.01–27.48	3.12–27.46
Goodness-of-fit on F^2	1.187	1.383
R_1, wR_2 ($I > 2\sigma(I)$)*	0.0385, 0.1028	0.0522, 0.1399
R_1, wR_2 (all data)*	0.0665, 0.1357	0.0832, 0.1793
Parameters of refinement	802	265
$\Delta\rho_{max}/\Delta\rho_{min}$, e Å^{-3}	0.551/–0.869	1.640/–1.135

* $R_1 = \Sigma(|F_o|-|F_c|)/\Sigma|F_o|$, $wR_2 = [\Sigma w(F_o^2 - F_c^2)^2/\Sigma w(F_o^2)^2]^{1/2}$, and $w = [\sigma^2(F_o^2) + (aP)^2 + bP]^{-1}$, where $P = (F_o^2 + 2F_c^2)/3$; $a = 0.0667$ and $b = 0.0000$ (**I**); $a = 0.0461$ and $b = 2.0366$ (**II**).

Hbza)Cl]$_2$ complex molecule, the Cu atoms are pentacoordinated by N(1), N(2) atoms of the bidentate chelating Phen ligand, two μ_2-Cl$^-$ ions and one carboxylate O atom of *o*-hydroxybenzoate to complete distorted $CuON_2Cl_2$ square-pyramidal coordination with basal Cu–O 1.929–1.940, Cu–N 2.019–2.030, Cu–Cl 2.248, 2.283 Å and axial Cu–Cl 2.667, 2.775 Å. The τ values about Cu(1) and Cu(2) of 0.094 and 0.119 [20] together with the bonding parameters (Table 2) indicate the both of Cl_2N_2O polyhedra to be somewhat distorted square pyramid ones with the metal centers shifted by 0.076(1) and 0.099(1) Å, respectively, from the basal plane towards the corresponding apex. The C–O bond lengths which the O atoms from *o*-hydroxybenzoate are coordinated in the region 1.265(4)–1.275(4) Å are longer than those which are not coordinated in the region 1.243(4)–1.247(4) Å. Additionally, the O(10) and O(11) aqua ligands from the mononuclear copper(II) structure form nearly linear intermolecular hydrogen bond O–H…O to the dissociative *o*-hydroxybenzoate carboxylate O(12) and O(13) with O···O 2.613 and 2.843 Å. The interplanar distance 3.579 Å between the Phen of the mononuclear copper(II) structure and the dinuclear structure indicates significant π···π stacking interactions making a contribution to formation of a trinuclear copper(II) structure.

The O(6) hydroxyl atom and O(10)$^{\#1}$ coordinated water donate the hydrogen atoms to the carboxylate oxygen atom O(8)$^{\#2}$ and bridging Cl(2) to form an

Table 2. Selected interatomic distances (Å) and bond angles (deg) for **I** and **II***

Bond	*d*, Å	Bond	*d*, Å	Bond	*d*, Å
		I			
Cu(1)– O(1)	1.929(2)	Cu(1)–N(1)	2.030(3)	Cu(1)–N(2)	2.022(2)
Cu(1)–Cl(1)	2.667(1)	Cu(1)–Cl(2)	2.283(1)	Cu(2)–O(4)	1.940(2)
Cu(2)–N(3)	2.024(3)	Cu(2)–N(4)	2.019(2)	Cu(2)–Cl(1)	2.248(1)
Cu(2)–Cl(2)	2.775(3)	Cu(3)–O(7)	1.988(2)	Cu(3)–O(10)	1.950(2)
Cu(3)–O(11)	2.145(2)	Cu(3)–N(5)	2.007(3)	Cu(3)–N(6)	2.050(3)
		II			
Cu–O(1)	1.948(3)	Cu–O(4)	1.964(3)	Cu–N(1)	2.008(4)
Cu–N(2)	2.009(4)	Cu–Cl	2.616(2)		
Angle	ω, deg	Angle	ω, deg	Angle	ω, deg
		I			
O(1)Cu(1)N(1)	169.57(9)	O(1)Cu(1)N(2)	91.00(10)	O(1)Cu(1)Cl(1)	92.41(7)
O(1)Cu(1)Cl(2)	93.58(7)	N(1)Cu(1)N(2)	81.57(10)	N(1)Cu(1)Cl(2)	93.69(8)
N(1)Cu(1)Cl(1)	94.71(7)	N(2)Cu(1)Cl(1)	88.64(7)	N(2)Cu(1)Cl(2)	175.18(8)
Cl(1)Cu(1)Cl(2)	92.65(3)	Cu(2)Cl(1)Cu(1)	90.00(3)	O(4)Cu(2)N(3)	168.36(9)
O(4)Cu(2)N(4)	91.32(10)	O(4)Cu(2)Cl(1)	92.56(7)	N(3)Cu(2)N(4)	81.65(10)
N(3)Cu(2)Cl(1)	94.16(8)	N(4)Cu(2)Cl(1)	175.52(8)	O(7)Cu(3)O(10)	95.38(9)
O(7)Cu(3)O(11)	104.88(9)	O(7)Cu(3)N(5)	90.96(9)	O(7)Cu(3)N(6)	142.16(9)
O(10)Cu(3)O(11)	92.77(10)	O(10)Cu(3)N(5)	171.89(10)	O(10)Cu(3)N(6)	90.89(10)
O(11)Cu(3)N(5)	90.47(10)	O(11)Cu(3)N(6)	112.06(9)	N(5)Cu(3)N(6)	81.00(10)
Cl(1)Cu(2)Cl(2)	90.61(9)				
		II			
O(1)CuO(4)	93.88(15)	O(1)CuN(1)	90.02(15)	O(1)CuN(2)	169.55(16)
O(1)CuCl	94.74(13)	O(4)CuN(1)	167.15(17)	O(4)CuN(2)	92.30(16)
O(4)CuCl	96.78(14)	N(1)CuN(2)	82.19(16)	N(1)CuCl	95.09(12)
N(2)CuCl	92.89(13)				

intermolecular hydrogen bonds O–H···O and O–H···Cl with O(6)···O(8) 3.17 and O(10)···Cl(2) 3.24 Å. Due to this type of interactions, the molecules are assembled into 1D supramolecular chains $^{1}_{\infty}\{[Cu(Phen)(o\text{-}Hbza)Cl]_2[Cu(Phen)(o\text{-}Hbza)(H_2O)_2]\}$ along [001] direction with the chelating Phen ligands extending parallely outwards on both sides (Fig. 2a). The Phen ligands of one chain intrude into the void space between the Phen ligands of the adjacent supramolecular chains with the interplanar Phen-to-Phen distances varying over the range 3.72 to 3.75 Å, indicating strong π···π stacking interactions. As a result, the intercalation of the Phen ligands of the supramolecular chains leads to 2d layers parallel to (100) as shown in Fig. 3. Obviously, the π···π stacking interactions are contributing to form the 2D layers assembly of the chains into layer parallel to (001).

The asymmetric unit of **II** contains one Cu^{2+} ion, one Phen molecule, one Cl^- anion, one water molecule, and one *p*-Hbza anion. As illustrated in Fig. 1b, *p*-Hbza ion functions as monodentate ligand providing one carboxylic O(1) atom to coordinate one Cu^{2+} ion. The each of Cu^{2+} ions is coordinated by N(1), N(2) atoms of one Phen molecule, O(1), O(4) atoms from one *p*-Hbza ion and one H_2O molecule, respectively, and one Cl^- anion, building up a square pyramidal $CuClN_2O_2$ coordination environment with N(1), N(2), O(1), and O(4) atoms at the corners of the basal plane and Cl atom at the apical position. The Cu–N bond distances range from 2.008(4) to 2.009(4) Å, while Cu–O bond lengths fall in the range 1.948(3)–1.964(3) Å (Table 3). The cisoid bond angles around

Table 3. Hydrogen bonding contacts for **I** and **II***

D–H···A	Distance, Å			Angle DHA, deg
	D–H	H···A	D···A	
		I		
O(3)–H(3*B*)···O(12)$^{\#1}$	0.83	2.22	3.048(6)	179
O(6)–H(6*B*)···O(8)$^{\#2}$	0.80	2.36	3.161(4)	179
O(9)–H(9*B*)···O(8)	0.82	1.78	2.506(4)	147
O(10)–H(101)···Cl(2)$^{\#3}$	0.97	2.27	3.242(6)	179
O(10)–H(102)···O(12)	0.81	1.80	2.613(4)	178
O(11)–H(111)···O(13)	0.85	1.99	2.843(5)	179
O(11)–H(112)···O(8)	0.70	2.25	2.928(5)	164
O(14)–H(14*A*)···O(12)	0.82	1.79	2.516(4)	148
		II		
O(3)–H(31)···Cl$^{\#1}$	0.94	2.15	3.089(4)	180
O(4)–H(41)···O(1)	0.82	2.41	2.858(6)	115
O(4)–H(41)···O(2)	0.82	1.73	2.541(5)	167
O(4)–H(42)···O(5)	0.82	1.93	2.710(4)	158
O(5)–H(51)···Cl$^{\#2}$	0.85	2.36	3.189(6)	168
O(5)–H(52)···Cl$^{\#3}$	0.83	2.36	3.138(4)	157

* Symmetry transformations used to generate equivalent atoms: for **I**—$^{\#1}$ $x, -y + 1/2, z + 1/2$; $^{\#2}$ $x, y + 1, z$; $^{\#3}$ $x, -y + 1/2, z - 1/2$; for **II**—$^{\#1}$ $-x + 2, -y + 1, -z + 2$; $^{\#2}$ $-x + 1, -y + 1, -z + 1$; $^{\#3}$ $x - 1, y, z$.

Cu^{2+} ion fall in the range 82.19°–93.88°, and the transoid ones are 167.15° and 169.55°, exhibiting significant departure from the corresponding value for a regular square pyramid (90° and 180°). The coordination sphere of copper(II) is best described from the τ value of 0.04 [20], which indicates that coordination polyhedron of Cu(II) is a square pyramid. The complex molecules display significant intramolecular hydrogen bond from the dissociated aqua ligand to the coordinating aqua O(4) atom. The O(3) hydroxyl atom coordinated to Cu donates its H to the Cl^- to form a nearly linear hydrogen bond with O(3)–H···Cl$^{\#1}$ 3.089 Å and angle O(3)–H···Cl$^{\#1}$ 179° ($^{\#1}$ $-x + 2, -y + 1, -z + 2$). Through these intermolecular hydrogen bonds, the adjacent molecules are paired to generate hydrogen-bonded centrosymmetric dinuclear motifs (Fig. 4). The mean interplanar distances between neighboring dinuclear units of the benzene ring is of 3.35 Å, suggesting a significant intermolecular face-to-face π···π stacking interactions. Such intermolecular interactions are regarded as the driving forces to assemble dinuclear molecules inter 1D supramolecular layer (Fig. 2b). The lattice O(5) water molecule donates two hydrogen atoms to form an interlayer hydrogen bonds O–H···Cl to the adjacent Cl^- of a adjoining molecule with O(5)···Cl$^{\#2}$ 3.189, O(5)···Cl$^{\#3}$ 3.138 Å and angles O(5)–H···Cl$^{\#2}$ 168°, O(5)–H···Cl$^{\#3}$ 157° ($^{\#2}$ $-x + 1, -y + 1, -z + 1$, $^{\#3}$ $x - 1, y, z$), which expand the 1D chains to 2D supramolecular layers parallel to (010) (Fig. 5), and the 2D layers finlly form 3D network structure via C–H···O weak hydrogen bonds.

The IR spectra of the title complexes give features attributable to each component of the complexes, which are compatible with the structural characteristics (see below). The absorption bands in the region 3700–3000 cm^{-1} for **I** are obviously due to the O–H stretching vibrations of the lattice water molecules and the *o*–hydroxybenzoate anions, and a broad band centered at 3169 cm^{-1} for **II**, which is diagnostic of the water molecules. The sharp, strong peaks at 1583 cm^{-1} for **I** and 1595 cm^{-1} for **II** are attributable to the ν_{as}(COO–) vibrations of the carboxylate groups of the *o*-hydroxybenzoate and *p*-hydroxybenzoate anions, while the medium-strong absorption due to the ν_s(COO–) vibrations is observed at 1389 cm^{-1} for both **I** and **II**. The wavenumber difference of 194 cm^{-1} for **I** and 206 cm^{-1} for **II** suggests that the carboxylate groups are in a monodentate coordination mode. According to the spectra of Phen and *o*-Hbza, the absorption peaks at 1485, 1450 cm^{-1} for **I** are

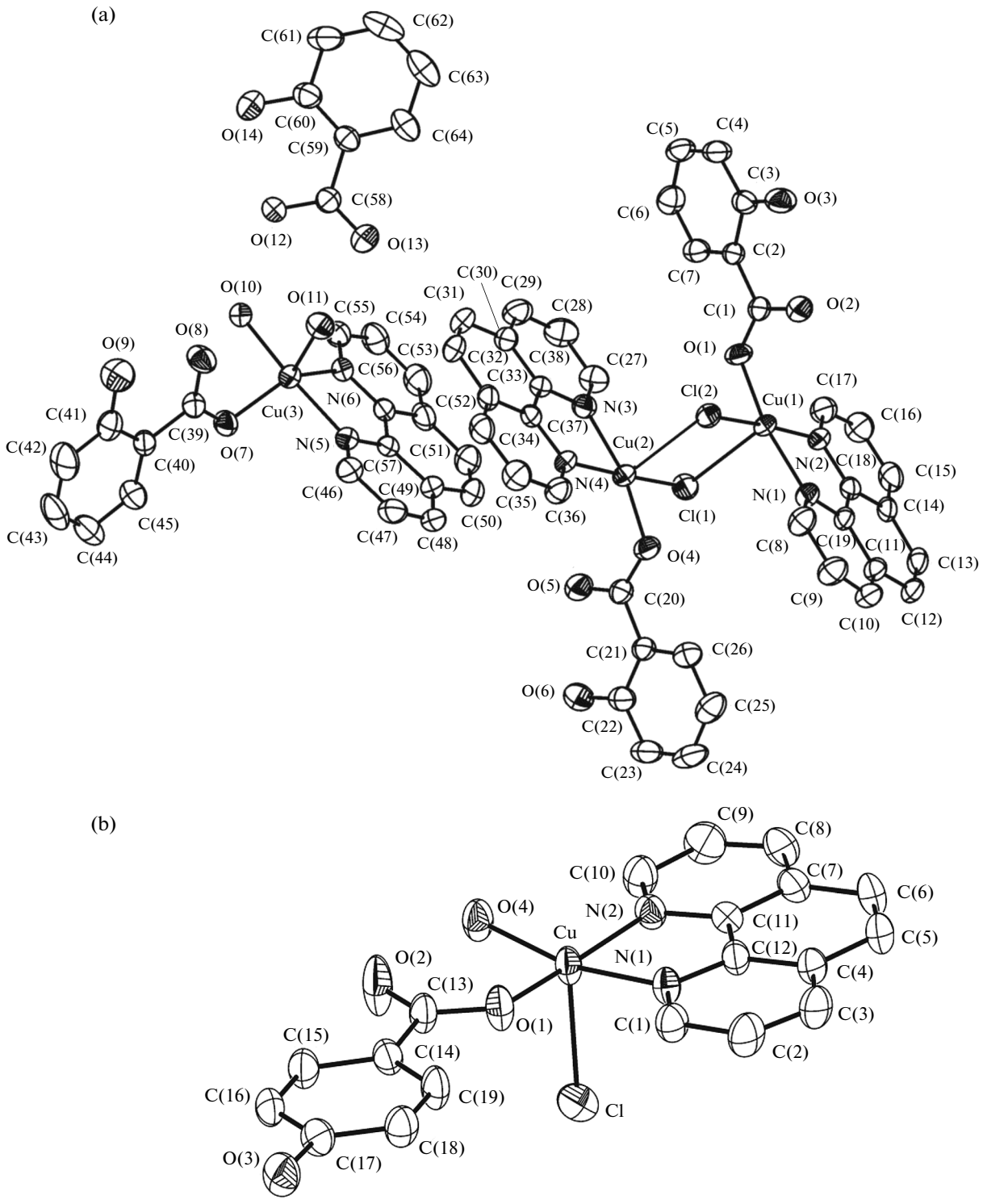

Fig. 1. Ortep view of the dinuclear complex **I** (a) and the mononuclear complex **II** (b) with displacement ellipsoids (45% probability) and atomic labeling.

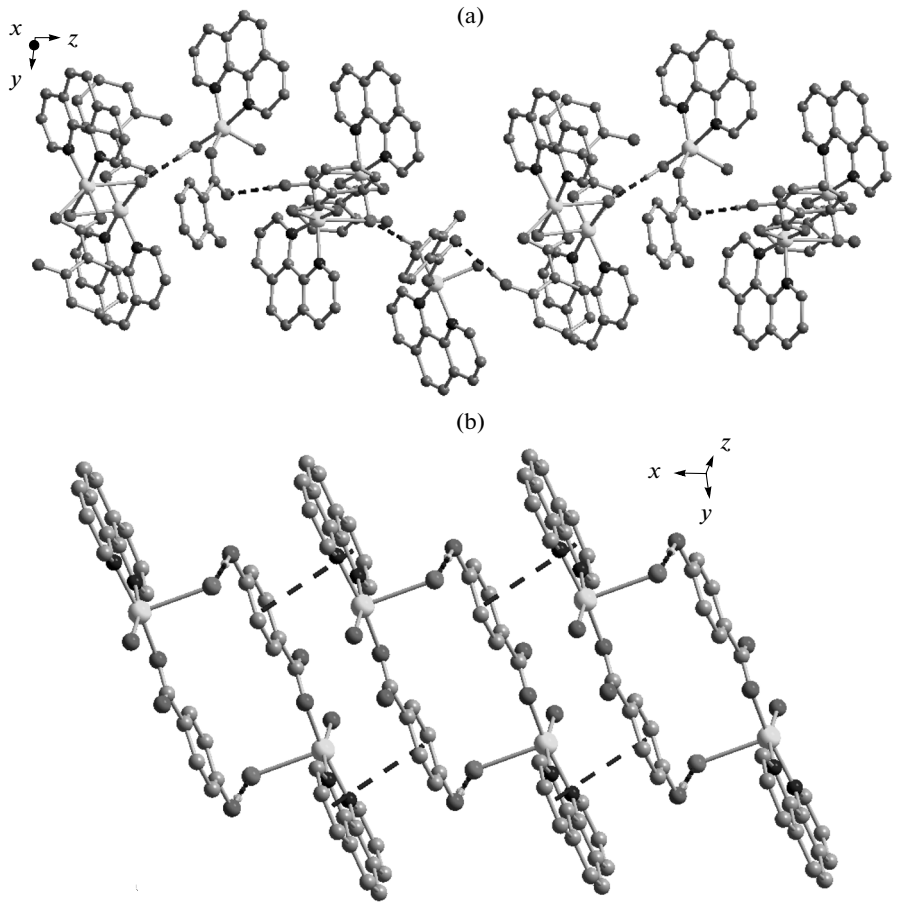

Fig. 2. Supramolecular assembly of **I** into 1D chains via intermolecular hydrogen bonds (a) and **II** into 1D chains via π···π stacking interactions (b).

assigned to the C=N and C=C vibrations of the pyridyl ring, and the ν(Ar–O) stretchings generate two absorption peaks at 1256 and 1220 cm^{-1}. The ν(C–H) stretching vibrations result in a weak absorption at 2924, 3065 cm^{-1} for **I** and 3022 cm^{-1} for **II**, and the out-of-plane C–H vibrations lead to absorptions at 852, 757, 721 cm^{-1} for **I** and 848, 789, 723 cm^{-1} for **II**, respectively. The absorptions due to Cu–O and Cu–Cl vibrations should appear below 550 cm^{-1} [21].

Thermal analyses (Fig. 6) shows **I** to be stable below 80°C, at which temperature decomposition starts. Weight loss at 140°C reaches 2.59% in good agreement with the value of 2.60% calculated for **II** due the removal of mole H_2O per formula, implying complete dehydration. The resulting anhydrous intermediate product [Cu(Phen)(*o*-Hbza)][Cu(Phen)(*o*-Hbza)Cl]$_2$(*o*-Hbza) undergoes a decomposition with the weight loss of 39.20% up to 300°C, due to the removal of two moles Phen per formula unit (calcd. 38.99%). Upon further heating, the resulting intermediate [Cu(*o*-Hbza)][Cu(*o*-Hbza)Cl]$_2$(*o*-Hbza) undergoes gradual decomposition and the collapse of organic skeleton. The final black solid residual of 25.26% was collected at 900°C. Thermogravimetric analysis of complex **II** shows that lattice and coordinated water molecule is readily eliminated from the network (calcd. 7.96%; found 7.15%) when the temperature is increased from room temperature to about 220°C. An abrupt weight loss from 230 to 900°C indicated decomposition of Phen and *p*-Hbza with weight loss of 69.94%. A final black solid residue of 24.36% is collected at 900°C.

Temperature-dependent magnetic susceptibility measurements for **I** and **II** were performed on the polycrystalline sample in the temperature range of 2–300 K in a fixed magnetic field 1000 G, and the $\chi_m T$ and χ_m (inset) versus T plots are shown in Fig. 7 (χ_m is the molar magnetic susceptibility for three Cu^{2+} ions). The magnetic behaviour of **I** reveals the room temperature $\chi_m T$ value of 1.127 $cm^3\ mol^{-1}$ K, which is in good agreement with the spin-only value of 1.125 $cm^3\ mol^{-1}$ K expected for three isolated Cu^{2+} ions ($S = 1/2$). Upon lowering the temperature, the $\chi_m T$ values gradually increases until at about 12 K, and then the value increases rapidly with decreasing temperature, reaching a maximum of 1.489 cm^3 K mol^{-1} at 2 K. The global feature is characteristic of significant ferromag-

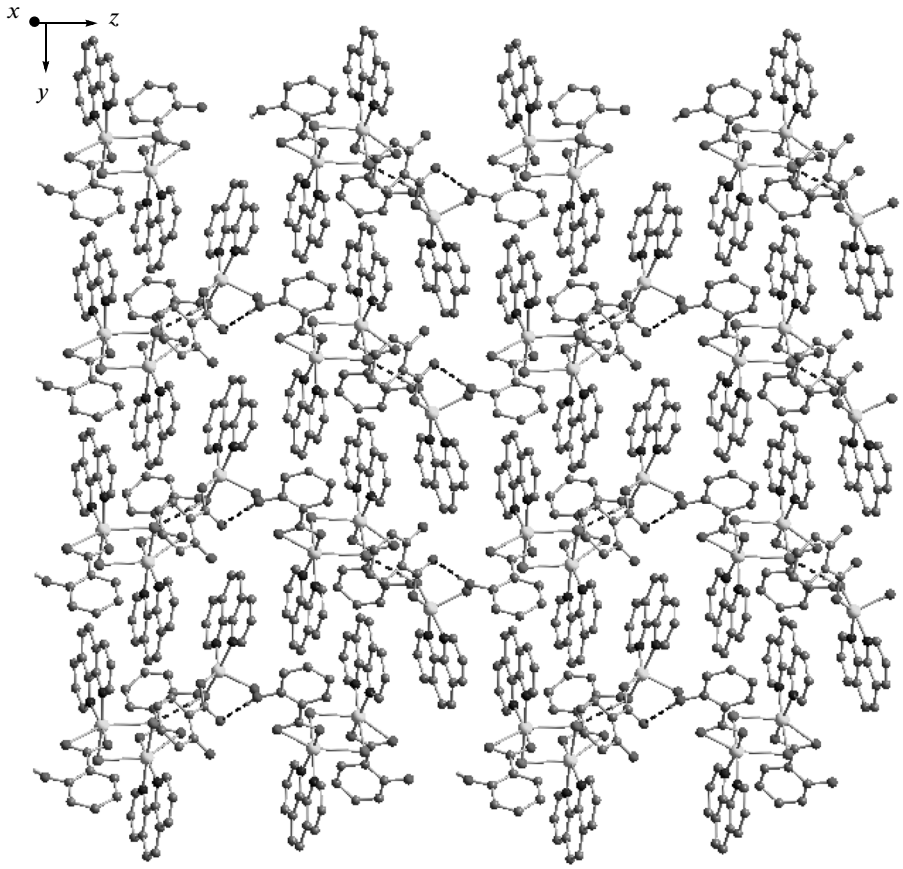

Fig. 3. 2D supramolecular layer of **I** formed by π···π stacking interactions.

netic coupling. The temperature-dependent magnetic susceptibility above 2 K follows the Curie–Weiss law $\chi_m = C/(T-\theta)$, and the best fit of the χ_m versus T plot gives a Curie constant $C = 1.283$ (2) cm^3 mol^{-1} K and Weiss constant $\theta = 0.284(4)$ K, suggesting the presence of weak ferromagnetic interaction among the Cu^{2+} ions. The magnetic behaviour of **I** will be in two parts of equation as follows [22], which the equation is contained the formula of the mononuclear Cu(II) unit and the binuclear Cu(II) unit.

$$\chi_{tri} = \chi_{mono} + \chi_{bi}, \quad (1)$$

$$\chi_{tri} = \frac{2N\beta^2g^2}{3kT}S(S+1) + \frac{2N\beta^2g^2}{3kT}\left[1+\frac{1}{3}\exp(-2J/KT)\right]^{-1}. \quad (2)$$

The Hamiltonian employed is $H = -JS_1S_2$ (where N is the Avogadro's number; g is the spectroscopic splitting factor; β is the Bohr magneton; k is the Boltzmann's constant; J is the exchange parameter). The expression in equation (2) was corrected using the molecular field approximation (equation (3)), to which the measured magnetic susceptibility data were fitted:

$$\chi_m = \frac{2N\beta^2g^2}{3kT}S(S+1) + \frac{\chi_{mono}}{1-\chi_{mono}(2zJ'/N\beta^2g^2)}, \quad (3)$$

where χ_m is the exchange coupled magnetic susceptibility actually measured, χ_{di} is also the magnetic susceptibility in the absence of the exchange field, zJ' is the total exchange parameter between Cu^{2+} ions (z is the number of nearest neighbors), and the rest of the parameters have their usual meanings. The best fit is

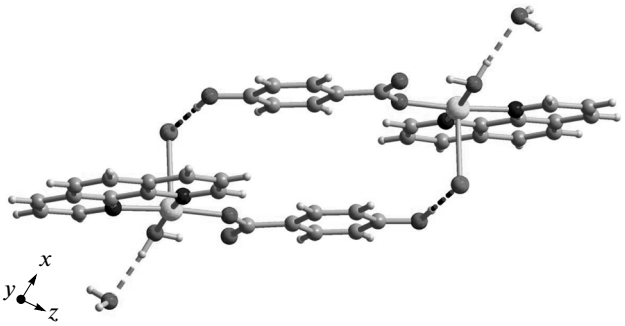

Fig. 4. The H-bonded dinuclear motifs assembled from a pair of adjacent mononuclear complex molecules in **II**.

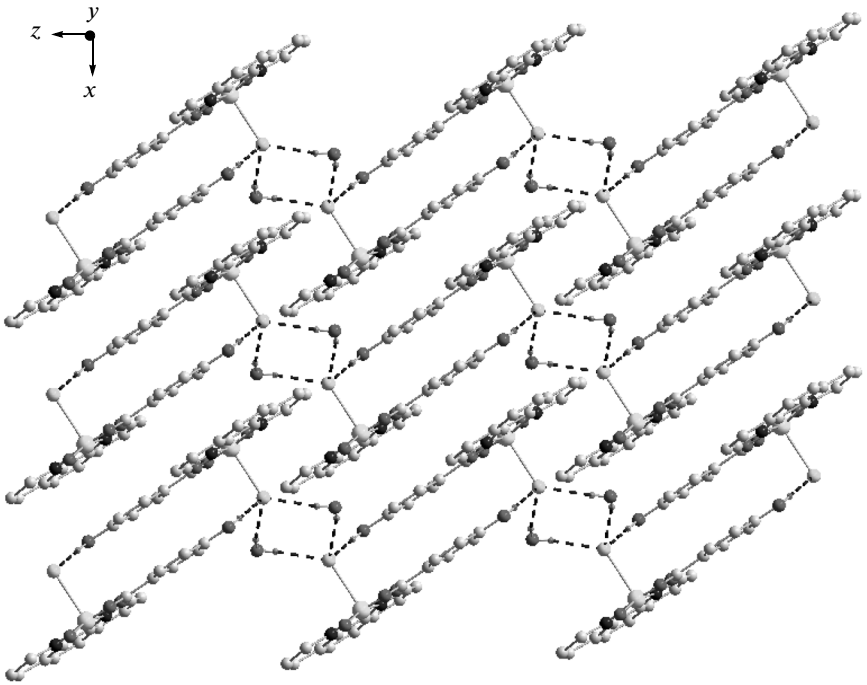

Fig. 5. Hydrogen bonding interactions assemble the chain into 2D supramolecular layers in **II**.

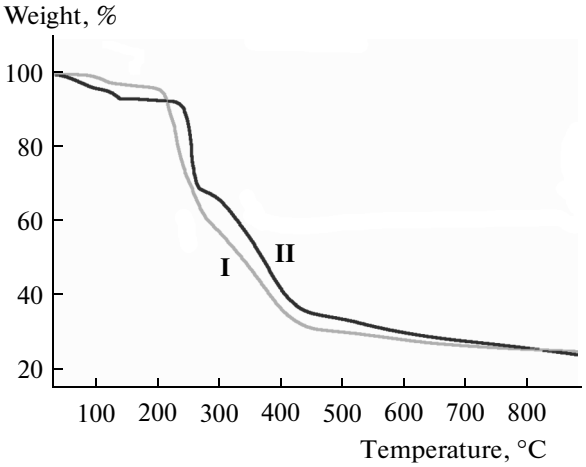

Fig. 6. Thermogravimetric curves for **I** and **II**.

obtained with values of $g = 1.933(1)$, $J = 63.58(9)$ cm^{-1}, $2zJ' = 0.196(4)$ cm^{-1}, and the agreement factor R is 5.0×10^{-5} ($R = \Sigma[(\chi_m)^{obs} - (\chi_m)^{calc}]^2/[(\chi_m)^{obs}]^2$). The positive J value suggests that the interactions between Cu^{2+} ions are ferromagnetic.

Complex **II** exhibits χ_m and $\chi_m T$ (inset) versus T plots similar to **I**. The value of $\chi_m T$ at room temperature equals 0.408 cm^3 K mol^{-1} and is a little higher than the spin-only value of 0.374 cm^3 K mol^{-1} expected for an uncoupled copper(II) ion. The fluctuation of magnetic susceptibility in low temperature range may be caused by zero-field splitting. The negative Weiss constant θ value of 0.040 K, obtained from the Curie–Weiss law within the measured temperature region, suggests the possibility of a very weak ferromagnetic interaction between magnetic centres inside crystal lattice via the non-covalent bond system in lower temperatures. In such situations, the exchange parameter zJ' can be determined only by a susceptibility equation with a molecular field correction. Therefore, in order to evaluate the intermolecular interac-

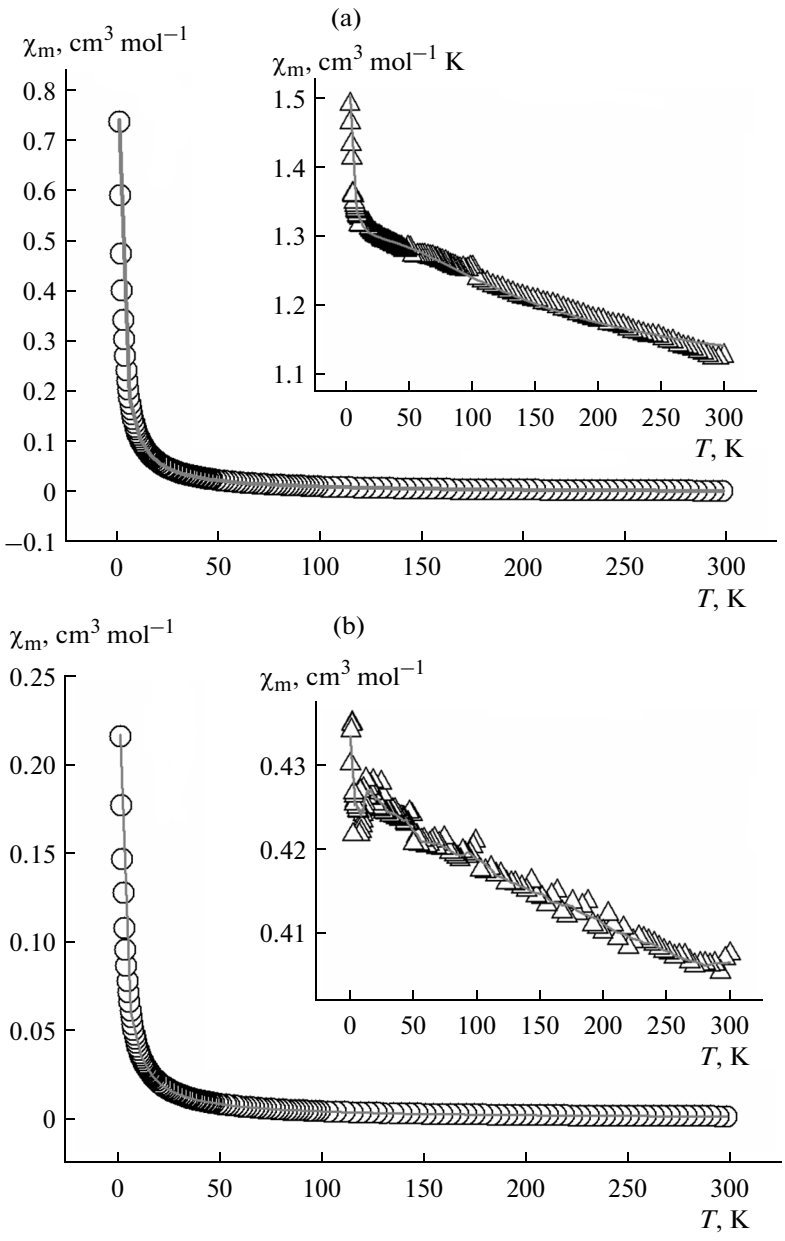

Fig. 7. Temperature dependence of the magnetic susceptibilities of **I** (a) and **II** (b). Solid lines represent the best fit.

tions of the magnetic centre of compound **II** a molecular exchange field model was used equation (5) [23].

$$\chi_m = \frac{2Ng^2\beta^2}{3kT}S(S+1), \quad (4)$$

$$\chi'_m = \frac{\chi_m}{(1 + 2zJ'\chi_m/Ng^2\beta^2)}, \quad (5)$$

where χ_m is the equation for the magnetic susceptibility of paramagnetic center; χ'_m is the measured experimental susceptibility; zJ' is the intermolecular exchange parameter; z is the number of nearest neighbors. In the frame of this model, the best-fit parameters obtained by the least-squares fit are the following: $zJ' = 0.055$ cm^{-1}, $g = 2.127$ with the value of $R = 9.5 \times 10^{-8}$, where R is the agreement factor defined as $R = \Sigma[(\chi_m)^{obs} - (\chi_m)^{calc}]^2/[(\chi_m)^{obs}]^2$.

ACKNOWLEDGMENTS

This project was sponsored by K.C. Wong Magna Fund in Ningbo University and supported by the Scientific Reaearch Fund of Zhejiang Provincial Education Department.

REFERENCES

1. Mamula, O. and Zelewsky, A.V., *Coord. Chem. Rev.*, 2003, vol. 242, p. 87.
2. *Coordination Polymers: Design, Analysis and Applications,* Batten, S.R., Neville, S.M., and Turner, D.R., Eds., Cambridge: RSC, 2009.
3. Sangeetha, N.M. and Maitra, U., *Chem. Soc. Rev.*, 2005, vol. 34, p. 821.
4. Corma, A., Rey, F., Rius, J., et al., *Nature*, 2004, vol. 431, p. 287.
5. Schmitt, W., Baissa, E., Mandel, A., et al., *Angew. Chem. Int. Ed.*, 2001, vol. 40, p. 3577.
6. Sozzani, P., Bracco, S., Comotti, A., et al., *Angew. Chem. Int. Ed.,* 2005, vol. 44, p. 1816.
7. Campidelli, S., Brandmuller, T., Hirsch, A., et al., *Chem. Commun.*, 2006, p. 4282.
8. Petitjean, A., Puntoriero, F., Campagna, S., et al., *Eur. J. Inorg. Chem.*, 2006, p. 3878.
9. Desiraju, G.R., *Acc. Chem. Res.*, 1996, vol. 29, p. 441.
10. Desiraju, G.R., *Acc. Chem. Res.*, 2002, vol. 35, p. 565.
11. Desiraju, G.R., *Angew. Chem. Int. Ed.*, 2007, vol. 46, p. 8342.
12. Fan, E., Vicent, C., Geib, S.J., and Hamilton, A.D., *Chem. Mater.*, 1994, vol. 6, p. 1113.
13. Garcia-Garibay, M.A., *Angew. Chem. Int. Ed.*, 2007, vol. 46, p. 8945.
14. Stang, P.J. and Olenyuk, B., *Acc. Chem. Res.*, 1997, vol. 30, p. 502.
15. Lemoine, P., Viossat, B., Morgant, G., et al., *J. Inorg. Biochem.*, 2002, vol. 89, p. 18.
16. Korah, R., Kalita, L., and Murugavel. R., *Indian J. Chem., Sect. A: Inorg., Bio-Inorg., Phys., Theor. Anal. Chem.*, 2011, vol. 50, p. 763.
17. Bain, G.A. and Berry, J.F., *J. Chem. Educ.*, 2008, vol. 85, p. 532.
18. Sheldrick, G.M., *SHELXS-97, Program for Crystal Structure Solution*, Göttingen (Germany): Univ. of Göttingen, 1997.
19. Sheldrick, G.M., *SHELXL-97, Program for Crystal Structure Refinement*, Göttingen (Germany): Univ. of Göttingen, 1997.
20. Addison, A.W. and Rao, N., *Dalton Trans.*, 1984, p. 1349.
21. Nakamoto, K., *Infrared and Raman Spectra of Inorganic and Coordination Compounds*, New York: Interscience-Wiley, 1986.
22. Campbell, G.C. and Haw, J.F., *Inorg. Chem.*, 1998, vol. 27, p. 3706.
23. Ginsberg, A.P. and Lines, M.E., *Inorg. Chem.*, 1972, vol. 11, p. 2289.